

VLM-Guided Group Preference Alignment for Diffusion-based Human Mesh Recovery

Wenhao Shen¹ Hao Wang^{2†} Wanqi Yin³ Fayao Liu⁴ Xulei Yang⁴

Chao Liang¹ Zhongang Cai³ Guosheng Lin^{1†}

¹Nanyang Technological University ²HKUST(GZ) ³SenseTime Research ⁴A*STAR

Abstract

Human mesh recovery (HMR) from a single RGB image is inherently ambiguous, as multiple 3D poses can correspond to the same 2D observation. Recent diffusion-based methods tackle this by generating various hypotheses, but often sacrifice accuracy. They yield predictions that are either physically implausible or drift from the input image, especially under occlusion or in cluttered, in-the-wild scenes. To address this, we introduce a dual-memory augmented HMR critique agent with self-reflection to produce context-aware quality scores for predicted meshes. These scores distill fine-grained cues about 3D human motion structure, physical feasibility, and alignment with the input image. We use these scores to build a group-wise HMR preference dataset. Leveraging this dataset, we propose a group preference alignment framework for finetuning diffusion-based HMR models. This process injects the rich preference signals into the model, guiding it to generate more physically plausible and image-consistent human meshes. Extensive experiments demonstrate that our method achieves superior performance compared to state-of-the-art approaches.

1. Introduction

This paper aims to tackle the challenge of monocular human mesh recovery (HMR), which involves estimating both human pose and shape from a single RGB image. Accurate 3D human perception is crucial for understanding activities and enabling applications such as VR, robotics, and gaming. However, this task is inherently ill-posed, as lifting 2D observations to 3D motion is highly ambiguous.

Specifically, optimization-based methods [6, 23, 41] iteratively refine human pose and shape from 2D cues, while regression-based approaches [18, 40, 45, 59] directly predict a single mesh per image. Both struggle with the ambiguity of lifting 2D to 3D, especially under occlusion or depth uncertainty. In contrast, probabilistic meth-

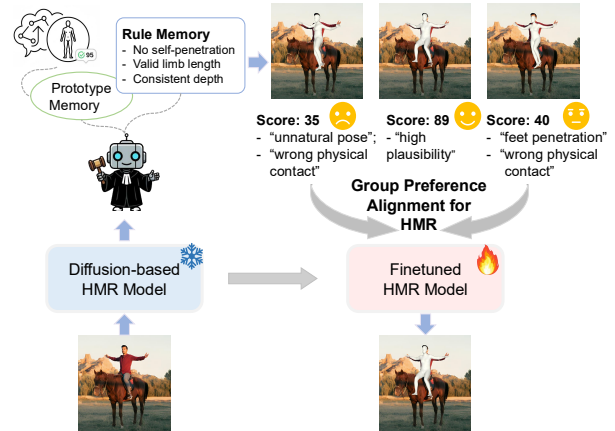


Figure 1. We introduce a VLM-guided HMR critique agent equipped with a dual-memory mechanism that delivers stable and semantically grounded assessments for groups of estimated 3D meshes. Building on these group-wise signals, our group preference alignment framework steers diffusion-based HMR models towards more coherent and reliable mesh generation.

ods [16, 28, 47, 50, 61] model this uncertainty via multiple predictions but often sacrifice accuracy for diversity.

It is observed that diffusion-based HMR methods [17, 61] often produce 3D meshes inconsistent with the 2D input, due to the lack of explicit 3D joint re-projection constraints. ADHMR [50] addresses this with Direct Preference Optimization (DPO), using a scorer to rank prediction quality. However, the image-driven scorer can be misled, favoring silhouette-aligned but physically implausible poses. In challenging scenarios, such as occlusion or incorrect contacts (e.g., floating feet, self-penetration), DPO often provides unreliable guidance. This is because DPO relies only on pairwise comparisons and ignores the quality relationships among multiple predictions.

In this work, we propose a comprehensive framework that utilizes a Visual Language Model (VLM)-based critique agent to improve the performance of the diffusion-based HMR model, as illustrated in Fig. 1. We observe that large VLMs already encode strong priors about human pose semantics, contact relations, and spatial consistency,

[†]Corresponding authors.

enabling them to assess the physical and geometric plausibility of 3D reconstructions from a single image. However, because of the criteria drift and subjective biases [30, 48], their raw judgments often lead to inconsistent or incomparable scores between prediction samples. To address this, we introduce a dual-memory augmented critique agent that can actively retrieve and reflect. In the exploration phase, it performs self-reflection to mine new judging rules and typical prediction prototypes, thereby refining its reasoning. During the evaluation phase, memory updates are disabled. The critique agent automatically retrieves relevant judging rules and prototype examples from its memory to ground each evaluation, yielding stable and semantically aligned assessments under occlusion or complex scene contexts.

Then, we aim to transfer the rich knowledge embedded in the critique agent to the human mesh estimator. Inspired by the success of Group Relative Policy Optimization (GRPO) [19, 49] in aligning large language models, we adapt its group-wise preference learning to diffusion-based HMR. However, applying GRPO to diffusion is challenging because GRPO relies on stochastic rollouts, whereas diffusion models typically rely on deterministic ODE samplers for better efficiency and quality [38, 51]. Prior attempts [36, 62] introduce stochasticity via SDE sampling but require training along the entire diffusion trajectory, increasing computation cost and reducing output fidelity.

We keep the efficiency of ODE-based diffusion and focus on the key benefit of GRPO, which is learning from group-level preference signals. Specifically, for each image, we generate several mesh hypotheses, score them with the critique agent, and convert these scores into advantages that capture their relative quality. Using these advantages, we formulate a simple and ODE-compatible group preference loss that transfers the critique agent’s judgment without requiring trajectory-level reinforcement. We find that this group-wise, advantage-weighted alignment enables the model to discern and refine subtle pose details, producing more semantically consistent results. Crucially, because our method relies on relative preference signals from the critique model, it remains effective even when finetuned on in-the-wild datasets with unreliable 3D annotations.

To summarize, our main contributions are:

- We propose a dual-memory augmented, self-reflective HMR critique agent to ensure consistent, semantically grounded scoring for human mesh predictions.
- We propose a group preference alignment framework for diffusion-based HMR models that operates without 3D ground truth. This design enables effective finetuning on noisy in-the-wild datasets and leads to more plausible and better 2D-aligned human mesh predictions.
- Extensive experiments show that this framework can effectively improve diffusion-based HMR models on challenging in-the-wild datasets.

2. Related Work

Human Mesh Recovery from a Single Image. Current HMR methods can be broadly divided into deterministic and probabilistic paradigms. Deterministic methods produce a single estimate for each input image. Early optimization-based approaches [6, 23, 29, 41] are time-consuming and often trapped in local minima due to poor initialization. More recent works [13, 18, 24, 31, 40, 45, 59] leverage deep neural networks to directly regress human model parameters, achieving strong performance yet still failing to address inherent depth and occlusion ambiguities in monocular settings. To tackle these ambiguities, probabilistic methods [3, 15, 28, 50, 61] aim to generate multiple predictions or model full posterior distributions. ScoreHypo [61] introduces a diffusion-based generator to produce diverse hypotheses and relies on an auxiliary selector network to choose the best estimate. ADHMR [50] uses Diffusion-DPO to align diffusion sampling with a learned HMR-Scorer. However, its 2D-based scorer is easily misled by occlusions and cluttered backgrounds. MEGA [16] explores stochastic generation through iterative token unmasking but remains limited by the expressiveness of its vector-quantized mesh codebook. In contrast, we extend GRPO to diffusion in an offline setting, using group-wise advantages to refine sampling and enhance fidelity.

Preference Learning for Diffusion Models. LLM alignment commonly uses Reinforcement Learning from Human Feedback (RLHF) [10], but it suffers from high cost and instability. While Direct Preference Optimization (DPO) [44] is simpler, it is often weaker. Recently, Group Relative Policy Optimization (GRPO) [19, 49] has emerged as a more stable and powerful framework, markedly improving LLM reasoning. Inspired by this success, recent studies have begun exploring aligning diffusion models. Early works [4, 11, 14, 60] follow the RLHF paradigm, while later efforts adapt DPO to diffusion [32, 34, 56, 63]. Only a few attempts explore GRPO for diffusion, hindered by the mismatch between GRPO’s stochastic exploration and the deterministic nature of ODE-based diffusion sampling. Recent works [36, 62] address this via SDE sampling, but at the cost of higher computation and slower convergence. Our method extends GRPO to diffusion in an offline setting, retaining both the stability of group optimization and the efficiency of standard diffusion models.

LLM as a Scorer. LLMs are increasingly used as scalable alternatives to expert judgment. Existing approaches include fine-tuned judges [21, 26, 58, 69], prompted judges [12, 33, 42], and multi-agent judges [8, 54, 66]. Fine-tuned models offer strong accuracy but often fail to generalize, prompted methods depend heavily on prompt design, and multi-agent pipelines are computationally expensive. We introduce the first VLM-enhanced scoring agent for HMR, equipped with dual memory and self-

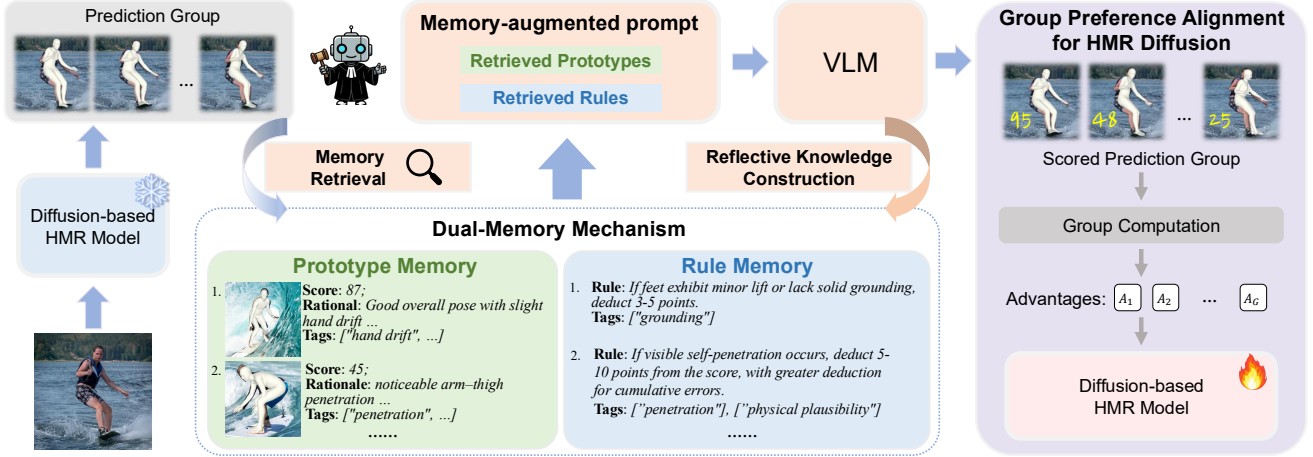


Figure 2. Overview of our framework. Our purpose is to refine a diffusion-based HMR model that generates a group of human mesh predictions per input image. We propose a VLM-enhanced HMR critique agent that assigns a score for each human mesh prediction. This critique agent is equipped with a dual-memory mechanism to give stable assessments. Then, we use this critique agent to build a group-wise HMR preference dataset without the need for manual labeling. Finally, we employ this preference dataset to finetune the base model to preferentially generate predictions that are physically plausible and better aligned with the image cues.

reflection to retrieve judging rules and visual prototypes, enabling consistent and semantically grounded evaluation without finetuning.

3. Method

3.1. Preliminaries

Diffusion Models. Diffusion models [20, 52] define a forward process that progressively adds Gaussian noise to clean data \mathbf{x} over T timesteps. In our setting, \mathbf{x} represents the joint swing and twist parameters following [31, 61], which are later converted into SMPL [37] pose parameters. The forward process follows $q(\mathbf{x}_t|\mathbf{x}_{t-1}) = \mathcal{N}(\sqrt{1-\beta_t}\mathbf{x}_{t-1}, \beta_t\mathbf{I})$, where the noisy sample can be expressed as $\mathbf{x}_t = \sqrt{\alpha_t}\mathbf{x}_0 + \sqrt{1-\alpha_t}\epsilon$, with $\epsilon \sim \mathcal{N}(0, \mathbf{I})$. The reverse process is modeled as

$$p_\theta(\mathbf{x}_{t-1}|\mathbf{x}_t) = \mathcal{N}(\mathbf{x}_{t-1}; \mu_\theta(\mathbf{x}_t, t), \sigma_t^2\mathbf{I}), \quad (1)$$

where β_t , α_t and σ_t are the noise schedules, μ_θ is computed from the noise prediction model ϵ_θ . The model is trained by minimizing a denoising loss:

$$L_{\text{DM}} = \mathbb{E}_{t, \mathbf{x}_0, \epsilon} [\lambda_t \|\epsilon - \epsilon_\theta(\mathbf{x}_t, t)\|_2^2], \quad (2)$$

where λ_t is a timestep weighting function. In the continuous-time view [52], the diffusion process is modeled as a stochastic differential equation (SDE), and its reverse-time SDE governs denoising. Removing the stochastic term yields a deterministic probability-flow ODE, which DDIM [51] leverages for faster, consistent sampling with the same trained model.

Group Relative Policy Optimization (GRPO). GRPO [49] extends Reinforcement Learning from

Human Feedback (RLHF) to a group-wise formulation, providing more stable policy updates while removing the need for a separate value model. For each condition c , a set of G samples $\{\mathbf{x}_0^i\}_{i=1}^G$ is generated from the old policy $p_{\theta_{\text{old}}}(\cdot|c)$. Formally, GRPO updates the policy parameters θ by maximizing the advantage-weighted likelihood ratio (we omit the clip term and KL term hereinafter for brevity):

$$\max_{\theta} \mathbb{E}_{c, \{\mathbf{x}_0^i\}} \left[\sum_{i=1}^G \frac{p_\theta(\mathbf{x}_0^i|c)}{p_{\text{ref}}(\mathbf{x}_0^i|c)} A(\mathbf{x}_0^i) \right], \quad (3)$$

where the advantage term is computed using a group of rewards $\{r_i\}_{i=1}^G$ corresponding to samples within the group:

$$A_i = \frac{r_i - \text{mean}(\{r_1, r_2, \dots, r_G\})}{\text{std}(\{r_1, r_2, \dots, r_G\})}. \quad (4)$$

3.2. Overview

An overview of our proposed framework is presented in Fig. 2. Given an input image I , we aim to predict the human pose parameters $\theta \in \mathbb{R}^{24 \times 3}$ and shape parameters $\beta \in \mathbb{R}^{10}$ of the SMPL model [41]. Following [61], we formulate this problem using a reverse diffusion process conditioned on the input image features c to tackle the inherent reconstruction ambiguity. We first propose a VLM-guided critique agent to assess the quality of human mesh predictions given an input image in Sec. 3.3. Next, we construct a synthetic group-wise HMR preference dataset (Sec. 3.4). Candidate human mesh predictions are generated by the reference model ϵ_{ref} and then grouped based on scores provided by the critique agent. To distill knowledge from this synthetic preference dataset, we propose a group-wise preference optimization framework that finetunes an HMR diffu-

sion model ϵ_θ to preferentially generate preferred human mesh predictions (Sec. 3.5), and ϵ_θ is initialized from ϵ_{ref} .

3.3. VLM-Guided HMR Critique Agent

To automate the nuanced task of evaluating HMR predictions, we introduce a VLM-guided HMR critique agent \mathcal{C}_{VLM} . Unlike traditional regressors that predict a score from 2D joint data [50], our agent emulates expert human judgment by working directly from rendered images. Formally, given an RGB image I and n human mesh prediction overlays $\{\hat{I}_j\}_{j=1}^n$ rendered on I , the agent outputs per-overlay scores $s_j \in [0, 100]$ and one-sentence critiques c_j .

The agent’s architecture combines a VLM scoring engine with a dual-memory mechanism and a self-reflective knowledge construction loop. It operates in two phases: an exploration phase to learn and build its memory, and an evaluation phase where this frozen knowledge is applied for consistent, robust scoring.

3.3.1. Dual-Memory Mechanism

The foundation of the agent is a VLM scoring engine guided by a dual-memory augmentation design. This design provides a lightweight yet interpretable prior that can be queried and expanded over time. Specifically, we use two different types of memory:

- **Rule Memory:** $\mathcal{M}_R = \{(t_i, T_i, N_i^u, N_i^s)\}_{i=1}^R$, where t_i is the assessment rule text, T_i is a set of semantic tags, N_i^u is a use count (tracking how often the rule has been applied), and N_i^s is a success count (tracking how often its application led to a ground-truth-aligned score).
- **Prototype Memory:** \mathcal{M}_P , stores previously judged hypothesis images as precedents. $\mathcal{M}_P = \{(v_i, r_i, T_i)\}_{i=1}^P$, where v_i is a visual embedding of the SMPL prediction overlay image using CLIP [43], and r_i is the textual rationale (including assigned score) for its assessment. T_i is a set of semantic tags.

Dual-memory augmented scoring. The dual-memory augmented scoring process is the agent’s core action, utilized in both the exploration and evaluation phases. It consists of three steps: (1) The agent queries prototype memory \mathcal{M}_P to retrieve the top- K most visually similar past examples by maximizing cosine similarity with the query image embedding v_q . (2) The agent queries \mathcal{M}_R using a hybrid score Ψ_j to select the most effective rules. This score combines semantic relevance (R) with UCB exploration (U):

$$\Psi_i = R(T_q, T_i) + U_i. \quad (5)$$

The Relevance Score, $R(T_q, T_i) = |T_q \cap T_i|$, rewards rules matching the query tags T_q from retrieved prototypes. The Upper Confidence Bound (UCB) [2] score is:

$$U_i = \rho_i + C \sqrt{\frac{\log N_{\text{total}}}{N_i^u + 1}}, \quad (6)$$

which balances the exploitation of high-success-rate rules and the exploration of rarely used rules. Here, $\rho_i = N_i^s / N_i^u$ is the historical success rate, C is an exploration constant, and $N_{\text{total}} = 1 + \sum_i N_i^u$ is the total number of rule applications. (3) Finally, a context-rich prompt is dynamically constructed, including the retrieved rules and prototype rationales. This prompt is fed to the VLM, which generates the final score s and critique c .

3.3.2. Reflective Knowledge Construction

We observe that while VLMs possess an inherent ability to judge 3D human mesh quality, direct prompting often yields unstable and inconsistent results. To this end, we allow the agent to build and refine domain-specific human pose estimation knowledge by itself in the exploration phase to stabilize its scoring capability.

The exploration phase is an iterative process where the agent’s primary goal is to populate its dual-memory by learning from ground-truth (GT) data: (1) The agent first performs the memory-augmented scoring process on a batch of data, which increments the use count N_i^u for every rule applied. (2) After scoring, it performs prototype memory write-back, saving salient examples back into \mathcal{M}_P . (3) The agent then performs an update for existing rules. It compares its score ranking against GT metrics via Spearman rank correlation. If the correlation is higher than a threshold τ , the applied rules are deemed effective, and their corresponding success count N_i^s is incremented, reinforcing their efficacy. (4) The core learning step is new rules mining via reflection. The agent instructs the VLM to inspect the discrepancy between its own output and the GT metrics and then propose 1-2 new, testable rules. These auto-mined rules are added to \mathcal{M}_R as new entries.

In the evaluation phase, the agent’s learning loop and memory are frozen. It exclusively performs the memory-augmented scoring to generate consistent, final evaluations on unseen data.

3.4. HMR Group Preference Dataset

To effectively train our mesh prediction policy using GRPO, we must first construct a dataset that provides richer supervision than standard pairwise preferences. However, manually annotating G complex 3D meshes is prohibitively slow, expensive, and subject to high inter-annotator variance. We overcome this bottleneck by leveraging our critique agent \mathcal{C}_{VLM} as a high-fidelity, automated annotator.

The dataset construction process follows two main stages: (1) **Group generation:** For each image I in our training corpus, we first require a diverse set of G human mesh predictions, $\{\mathbf{m}^i\}_{i=1}^G$. This set spans a wide range of qualities, from common failure modes to high-quality alignments. We generate this group by sampling our frozen, pre-trained diffusion-based HMR model, ϵ_{ref} for G times, conditioned on I but initiated with different initial noises. (2)

Group-wise scoring: We employ our critique agent \mathcal{C}_{VLM} to score the entire group of G predictions simultaneously to obtain consistent relative quality judgments within one group. The model is prompted with the image I and the complete set of mesh predictions $\{\mathbf{m}^i\}_{i=1}^G$ (visualized as 2D overlays) to get a set of scalar quality scores $\{s^i\}_{i=1}^G$:

$$\{s^1, \dots, s^G\} = \mathcal{C}_{\text{VLM}}(I, \mathbf{m}^1, \dots, \mathbf{m}^G). \quad (7)$$

By applying the scoring to all generated groups, we obtain our final, fully annotated group-wise preference dataset, \mathcal{G}_{HMR} . Each entry in this dataset is a tuple containing the input image, the group of predictions, and their corresponding VLM-assigned scores $\mathcal{G}_{\text{HMR}} = \{(I, (\mathbf{m}^1, s^1), (\mathbf{m}^2, s^2), \dots, (\mathbf{m}^G, s^G))\}$. This collection provides the dense preference signals $\{s^i\}$ required to train our GRPO refinement policy.

3.5. Group Preference Alignment for HMR

Once we obtain the group-wise preference dataset \mathcal{G}_{HMR} that encodes rich quality cues for HMR, we seek to instill this rich preference information into our diffusion model. While pairwise methods like Diffusion-DPO [50, 56] exist, probabilistic HMR models inherently generate multiple hypotheses to address the one-to-many mapping ambiguity. This multi-hypothesis approach necessitates a learning signal that is more stable and comprehensive than comparisons between isolated pairs. To this end, we introduce group preference alignment for HMR diffusion models. Our objective is to optimize a diffusion-based HMR estimator ϵ_θ , initialized from a reference denoiser ϵ_{ref} , such that it learns from the static group-wise HMR preference data and produces human mesh predictions that are more physically plausible and better aligned with image evidence.

Concretely, given the human mesh group preference dataset \mathcal{G}_{HMR} and the image condition \mathbf{c} , we follow GRPO (Eq. (4)) to compute the relative prediction quality advantage $A(\cdot)$ using their quality scores s^1, \dots, s^G :

$$A_i = \frac{s_i - \text{mean}(\{s_i\}_{i=1}^G)}{\text{std}(\{s_i\}_{i=1}^G)}. \quad (8)$$

Building on the GRPO objective in Eq. (3), which maximizes advantage-weighted likelihood ratios within each group, we treat the diffusion sampler as a conditional policy $p_\theta(\mathbf{m} | \mathbf{c})$ parameterized by the noise predictor ϵ_θ . Inspired by [44, 56], we then instantiate the group-wise update rule as an advantage-weighted log-likelihood ratio between the trainable policy p_θ and the frozen reference policy p_{ref} :

$$\mathcal{L}(\theta) = -\mathbb{E}_{\mathbf{c}, \{\mathbf{m}^i\}} \left[\sum_{i=1}^G A(\mathbf{m}^i) \log \frac{p_\theta(\mathbf{m}^i | \mathbf{c})}{p_{\text{ref}}(\mathbf{m}^i | \mathbf{c})} \right]. \quad (9)$$

To specialize this objective to diffusion-based HMR, we follow the reparameterization used in Diffusion-DPO [56]

and express the log-ratio through the corresponding diffusion paths $\mathbf{x}_{0:T}^i$:

$$\log \frac{p_\theta(\mathbf{m}^i | \mathbf{c})}{p_{\text{ref}}(\mathbf{m}^i | \mathbf{c})} \approx \mathbb{E}_{q(\mathbf{x}_{1:T}^i | \mathbf{m}^i)} \log \frac{p_\theta(\mathbf{x}_{0:T}^i)}{p_{\text{ref}}(\mathbf{x}_{0:T}^i)}, \quad (10)$$

where we approximate the intractable posterior over paths with the forward noising process $q(\mathbf{x}_{1:T}^i | \mathbf{m}^i)$. Under the standard Gaussian parameterization of the reverse diffusion process (Eq. (1)), p_θ is induced by the noise predictor ϵ_θ , and the log-likelihood ratio admits the following diffusion surrogate (we omit \mathbf{c} for brevity hereinafter):

$$\log \frac{p_\theta(\mathbf{m}^i | \mathbf{c})}{p_{\text{ref}}(\mathbf{m}^i | \mathbf{c})} \approx T \lambda_t \mathbb{E}_{t, \epsilon} \left[L_{\text{DM}}^{\text{ref}}(\mathbf{x}_t^i, \epsilon) - L_{\text{DM}}^\theta(\mathbf{x}_t^i, \epsilon) \right], \quad (11)$$

where $t \sim \mathcal{U}(\{1, \dots, T\})$, $\epsilon \sim \mathcal{N}(0, \mathbf{I})$, λ_t is a timestep weighting function, \mathbf{x}_t^i is obtained by diffusing \mathbf{m}^i , and

$$L_{\text{DM}}^\theta(\mathbf{x}_t^i, \epsilon) = \|\epsilon_\theta(\mathbf{x}_t^i, t) - \epsilon\|_2^2 \quad (12)$$

is the standard diffusion noise prediction loss (with an analogous definition for $L_{\text{DM}}^{\text{ref}}$). Plugging this surrogate into (9) yields our final training objective:

$$\mathcal{L}(\theta) = \mathbb{E}_{\mathbf{m} \sim \mathcal{G}_{\text{HMR}}, t \sim \mathcal{U}(1, T), \epsilon \sim \mathcal{N}(0, \mathbf{I})} \beta T \lambda_t \sum_{i=1}^G \left[A(\mathbf{m}^i) (L_{\text{DM}}^\theta(\mathbf{x}_t^i, \epsilon) - L_{\text{DM}}^{\text{ref}}(\mathbf{x}_t^i, \epsilon)) \right], \quad (13)$$

where the hyperparameter β controls regularization.

Intuitively, meshes with higher critique scores (positive advantages) are encouraged to achieve a smaller denoising loss than the reference model, while lower-scored meshes are pushed in the opposite direction, aligning the HMR diffusion model with the group-wise preference signal.

4. Experiments

4.1. Experimental Setup

Datasets. In the exploration phase, our critique agent samples images from five datasets: HI4D [64], BED-LAM [5], DNA-Rendering [9], GTA-Human II [7], and SPEC [27]. These studio-based or synthetic datasets provide accurate 3D ground-truth annotations across diverse scenes, offering reliable quality signals for building the agent’s knowledge. For the evaluation of the agent, we follow ADHMR [50] to construct our test sets. This involves using data from the DNA-Rendering [9] and GTA-Human II [7] test splits. For our reference diffusion model, we adopt the architecture from [50, 61] and train it on standard HMR datasets: Human3.6M [22], 3DPW [55], MPI-INF-3DHP [39], MPII [1], COCO [35], and UP-3D [29].

Metrics. We evaluate human mesh recovery using four standard metrics: PVE for mesh surface accuracy, MPJPE

	Methods	M	3DPW [55]			Human3.6M [22]			
			PVE ↓	MPJPE ↓	PA-MPJPE ↓	PVE ↓	MPJPE ↓	PA-MPJPE ↓	
Deterministic	HMR [24]	-	152.7	130.0	81.3	96.1	88.0	56.8	
	HybrIK [31]	-	86.5	74.1	45.0	65.7	54.4	34.5	
	PyMaf [67]	-	110.1	92.8	58.9	-	57.7	40.5	
	HMR 2.0 [18]	-	-	70.0	44.5	-	44.8	33.6	
	POTTER [68]	-	87.4	75.0	44.8	-	56.5	35.1	
	Zolly [57]	-	76.3	65.0	39.8	-	49.4	32.3	
	ScoreHMR [53]	-	-	76.8	51.1	-	-	-	
	CameraHMR [40]	-	65.9	56.0	35.1	-	-	-	
	PromptHMR [59]	-	69.4	58.7	36.6	-	-	-	
Probabilistic	3D Multibodies [3]	25	-	75.8	55.6	-	58.2	42.2	
	ProHMR [28]	25	-	-	52.4	-	-	36.8	
	Sengupta <i>et al.</i> [46]	25	-	75.1	47.0	-	-	-	
	HMDiff [17]	25	82.4	72.7	44.5	-	49.3	32.4	
	HuManiFlow [47]	100	-	65.1	39.9	-	-	-	
	ScoreHypo [61]	10	79.8	68.5	41.0	52.5	42.4	29.0	
		100	73.4	63.0	37.6	47.5	38.4	26.0	
	MEGA [16]	25	75.1	63.6	40.4	-	-	-	
		10	73.8	64.2	38.3	52.1	41.8	28.4	
	ADHMR [50]	100	65.4	57.2	33.5	45.9	36.9	24.8	
	Ours		10	69.0	59.3	36.3	49.5	39.6	27.2
			100	60.9	52.5	31.5	43.8	35.0	23.9
			200	59.0	51.0	30.2	42.4	34.0	23.2
	Ours[†]		10	67.2	56.6	36.4	49.2	39.0	26.9
			100	59.5	49.9	31.9	43.2	34.3	23.5
		200	57.7	48.5	30.5	42.0	33.2	22.8	

Table 1. Comparison with state-of-the-arts on the 3DPW [55] and Human3.6M [22] dataset. M is the number of predictions of probabilistic methods. Ours[†] is trained on an additional in-the-wild dataset InstaVariety [25], using only preference signals without 3D labels.

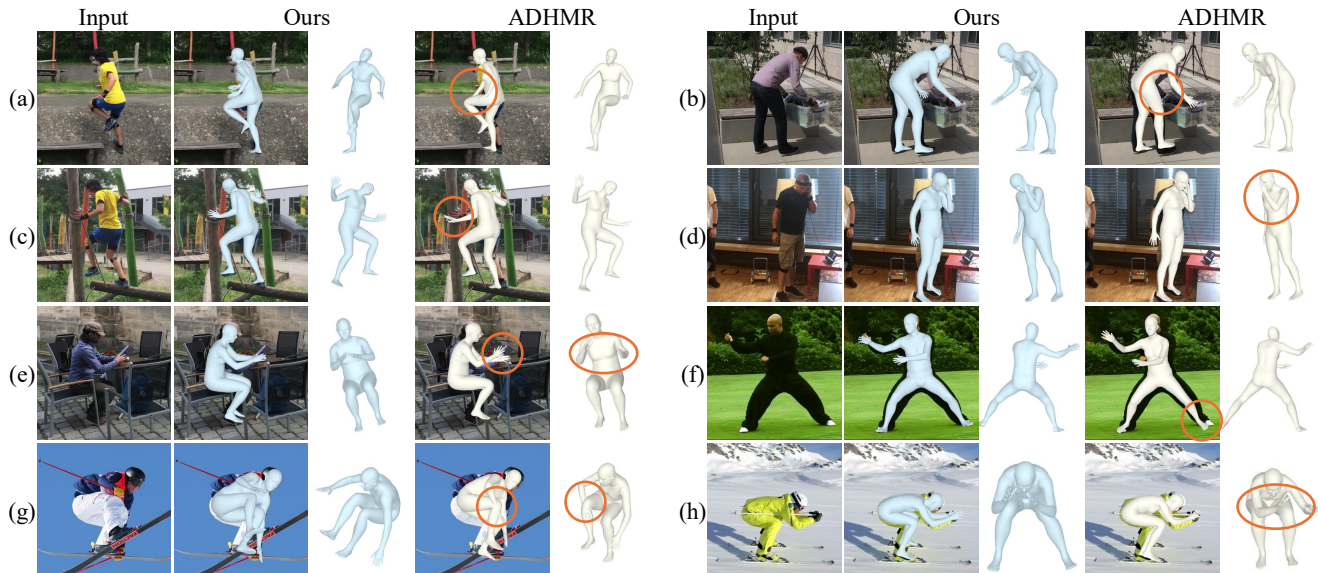


Figure 3. Qualitative comparison between our method and the state-of-the-art probabilistic model ADHMR [50]. Examples (a) ~ (e) are from the 3DPW [55] dataset, while (f) ~ (h) are challenging internet images. Both overlay and side-view results are shown.

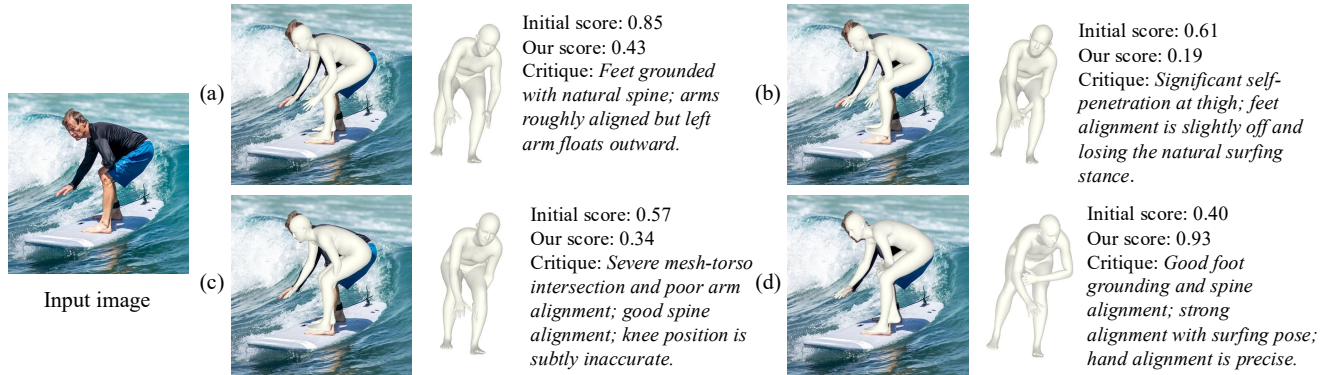


Figure 4. Visualization of our critique agent on an internet image. We compare the erroneous initial score from HMR-Scorer [50] with the corrected score from our critique agent, along with the corresponding critique.

Methods	3DPW [55]		
	PVE ↓	MPJPE ↓	PA-MPJPE ↓
Base Diffusion Model	73.4	63.0	37.6
+ supervised finetuning	70.2	61.3	36.5
Ours	59.5	49.9	31.9
DPO w/ critique agent	63.9	53.1	33.4
w/o critique agent	65.4	54.9	34.7

Table 2. Ablation study on the 3DPW [55] test set. All models are finetuned on the InstaVariety [25] dataset. $M = 100$ for all.

for 3D joint accuracy, and their Procrustes-aligned variants (PA-PVE and PA-MPJPE) that remove global misalignment. To evaluate our critique agent, we follow standard score-prediction protocols [50, 65] and compute three correlation metrics between predicted scores and ground-truth quality: PLCC for linear correlation, and SRCC and KRCC for rank-based consistency. Higher values (closer to 1.0) indicate better correlation.

Implementation details. We use Qwen3-VL-32B as our VLM in the critique agent. We use a learning rate of $1e^{-4}$ for the group preference finetuning with a batch size of 80 images. We use a group size of $G = 20$ for training.

4.2. Human Mesh Recovery Results

Quantitative comparison. Tab. 1 shows the comparison of our method with state-of-the-art methods on two widely used benchmark datasets: Human3.6M [22] and in-the-wild 3DPW [55]. Following standard conventions for probabilistic methods [3, 50, 61], we generate M estimates and report the minimum PVE, MPJPE, and PA-MPJPE. When fine-tuned directly on these benchmarks, our method significantly improves the reference model’s performance, demonstrating its ability to effectively leverage group-wise reward signals. Notably, on the 3DPW in-the-wild benchmark, our model achieves an 8.2% MPJPE improvement ($M = 100$) over ADHMR [50], even without using an additional in-the-wild dataset. To further evaluate in-the-wild effectiveness, we introduce a variant, Ours[†], which is fine-

tuned on the InstaVariety [25] dataset. Crucially, instead of using the dataset’s noisy pseudo 3D labels for a loss, we use its images to construct a new group-wise preference dataset via our critique agent and the frozen reference model. This approach allows our model to achieve superior results, surpassing the previous SOTA ADHMR [50]. This performance boost highlights the generalizability of our critique agent and the effectiveness of our group preference alignment framework in enhancing in-the-wild generalization.

Qualitative results. Fig. 3 compares our method with the state-of-the-art probabilistic method ADHMR on challenging samples from 3DPW and in-the-wild internet images. The results prove our model’s superior performance under severe occlusion and complex human-object interactions. In cases (a) and (b), our model recovers more plausible poses for the partially occluded arms and achieves better alignment with the input image. In (d), where the subject is making a phone call, ADHMR misestimates the depth relationship between the left arm and the head, whereas our model correctly places the arm near the face, reflecting stronger semantic and spatial reasoning. In (g), ADHMR generates self-penetration artifacts, while our result remains physically valid. In (h), despite heavy occlusion on the left side, our model still predicts a coherent 3D pose, whereas ADHMR falls into depth ambiguity. These results collectively demonstrate that our model is substantially more robust than ADHMR on challenging in-the-wild scenarios.

Ablation study. Tab. 2 presents our ablation study. All variants are fine-tuned on the in-the-wild InstaVariety [25] dataset and evaluated on the 3DPW [55] test set. The base diffusion model serves as our reference model, and we note that conventional supervised fine-tuning on noisy pseudo-labels provides only limited improvement. To assess the value of our group preference alignment framework, we compare it with a DPO-style pairwise variant following ADHMR [50], using the same critique agent for fairness. Compared with the DPO-based variant, our group preference alignment framework reduces the MPJPE error by

Methods	GTA-Human II [7]						DNA-Rendering [9]					
	PVE		MPJPE		PA-MPJPE		PVE		MPJPE		PA-MPJPE	
	SRCC \uparrow	KRCC \uparrow	SRCC \uparrow	KRCC \uparrow	SRCC \uparrow	KRCC \uparrow	SRCC \uparrow	KRCC \uparrow	SRCC \uparrow	KRCC \uparrow	SRCC \uparrow	KRCC \uparrow
ScoreNet [61]	0.464	0.411	0.468	0.404	0.430	0.327	0.532	0.512	0.496	0.469	0.458	0.367
HMR-Scorer [50]	0.578	0.506	0.588	0.513	0.489	0.428	0.610	0.540	0.562	0.508	0.475	0.393
Ours	0.605	0.539	0.615	0.556	0.528	0.461	0.633	0.556	0.588	0.532	0.510	0.433
<i>w/o rule memory</i>	0.597	0.491	0.577	0.480	0.454	0.427	0.619	0.487	0.564	0.520	0.484	0.377
<i>w/o prototype memory</i>	0.590	0.455	0.602	0.479	0.464	0.398	0.622	0.542	0.564	0.513	0.482	0.378
<i>w/o self-reflection</i>	0.534	0.426	0.542	0.444	0.440	0.285	0.568	0.463	0.567	0.460	0.483	0.298

Table 3. Group-wise score prediction results. We report the SRCC and KRCC between the predicted scores and the ground-truth HMR metrics. Our method consistently outperforms all baselines and ablation variants.

Methods	GTA-Human II [7] - PLCC			DNA-Rendering [9] - PLCC		
	PVE	MPJPE	PA-MPJPE	PVE	MPJPE	PA-MPJPE
ScoreNet [61]	0.524	0.516	0.472	0.550	0.551	0.499
HMR-Scorer [50]	0.634	0.627	0.565	0.664	0.659	0.620
Ours	0.695	0.697	0.653	0.737	0.717	0.700
<i>w/o rule memory</i>	0.683	0.672	0.630	0.701	0.673	0.650
<i>w/o prototype memory</i>	0.645	0.629	0.597	0.677	0.659	0.629
<i>w/o self-reflection</i>	0.610	0.613	0.540	0.642	0.656	0.581

Table 4. Point-wise score prediction results. We report the PLCC between the predicted scores and the ground-truth metrics.

6.0%, reflecting its stronger ability to leverage group-wise preference signals and mitigate the mapping ambiguity of probabilistic models. When removing the critique agent and using only the group alignment framework (*Ours w/o critique agent*), we rely on the HMR-Scorer [50] to build the preference dataset. This variant improves over the baseline but still lags behind our full model, highlighting the value of high-fidelity signals provided by the critique agent. Overall, the ablation results indicate that our performance gains arise from the combination of the critique agent’s richer supervision and the strong alignment capability of our method.

4.3. HMR Critique Agent Results

Evaluation protocol. To evaluate the critique agent, we use two protocols: point-wise and group-wise. Point-wise evaluation assesses the agent’s ability to predict the absolute quality of each single prediction, while group-wise evaluation tests its ability to rank the relative quality of K predictions for the same image. Our point-wise benchmark is identical to that of ADHMR, using single perturbed GT poses to simulate predictions. For group-wise evaluation, we generate K distinct predictions per image and compute correlation within each group, reporting the mean across groups. We calibrate the critique agent’s outputs to the HMR-Scorer’s numeric range using a quadratic programming post-processing step that learns a linear scale-and-shift transformation.

Group-wise results. Tab. 3 reports the group-wise score prediction results. We compare against two baselines: ScoreNet [61] and HMR-Scorer [50], both of which rely merely on joint-guided image features. Results show that our critique agent outperforms all baseline methods in both SRCC and KRCC metrics, indicating its stronger capability to capture subtle 3D pose variations. We further con-

duct ablations by removing each core component. *Ours w/o rule memory* removes the agent’s access to the learned rules, leading to weaker and less stable ratings. *Ours w/o prototype memory* removes instance-level prediction prototypes, which also degrades performance. *Ours w/o self-reflection* eliminates reflective knowledge construction in the exploration phase. This variant causes the most significant performance drop across all metrics, strongly underscoring that the self-reflection process is a critical component for enhancing the ranking stability of the agent.

Point-wise results. Tab. 4 presents the point-wise score prediction results. The ablations further validate our design: removing either the rule memory or the prototype memory causes a noticeable performance drop, showing that both general rules and instance-level prototypes are important for accurate quality prediction. The self-reflection mechanism is also essential, as its removal leads to the largest decline, confirming its role in producing reliable scores.

Visualization. Fig. 4 illustrates the clear advantages of our critique agent over the HMR-Scorer baseline. The baseline’s “Initial score” is unreliable and appears to lack 3D awareness: it assigns a high score to a flawed pose (a) and an incorrectly low score to a high-quality 3D mesh (d). In contrast, our critique agent demonstrates a robust comprehension of the 3D action and geometry. It correctly identifies that poses (a) and (c) fail to capture the proper surfing stance, especially the incorrectly extended left arm. Our agent also identifies major 3D geometric failures such as severe self-penetration (b, c). This shows our agent’s feedback is grounded in a precise understanding of 3D human motion, allowing it to identify subtle errors, thus rectifying the base model’s flawed assessments via our group preference optimization framework.

5. Conclusion

In this work, we introduce a VLM-driven critique agent and a group preference alignment framework that together align diffusion-based HMR. By providing semantically grounded preferences and learning from them without 3D supervision, our method produces more accurate human meshes, especially in challenging in-the-wild settings.

References

- [1] Mykhaylo Andriluka, Leonid Pishchulin, Peter Gehler, and Bernt Schiele. 2d human pose estimation: New benchmark and state of the art analysis. In *Proceedings of the IEEE Conference on Computer Vision and Pattern Recognition*, pages 3686–3693, 2014. 5
- [2] Peter Auer, Nicolo Cesa-Bianchi, and Paul Fischer. Finite-time analysis of the multiarmed bandit problem. *Machine learning*, 47(2):235–256, 2002. 4
- [3] Benjamin Biggs, David Novotny, Sebastien Ehrhardt, Hanbyul Joo, Ben Graham, and Andrea Vedaldi. 3d multi-bodies: Fitting sets of plausible 3d human models to ambiguous image data. *Advances in neural information processing systems*, 33:20496–20507, 2020. 2, 6, 7
- [4] Kevin Black, Michael Janner, Yilun Du, Ilya Kostrikov, and Sergey Levine. Training diffusion models with reinforcement learning. In *The Twelfth International Conference on Learning Representations*, 2024. 2
- [5] Michael J Black, Priyanka Patel, Joachim Tesch, and Jionglong Yang. Bedlam: A synthetic dataset of bodies exhibiting detailed lifelike animated motion. In *Proceedings of the IEEE/CVF Conference on Computer Vision and Pattern Recognition*, pages 8726–8737, 2023. 5
- [6] Federica Bogo, Angjoo Kanazawa, Christoph Lassner, Peter Gehler, Javier Romero, and Michael J Black. Keep it smpl: Automatic estimation of 3d human pose and shape from a single image. In *Computer Vision—ECCV 2016: 14th European Conference, Amsterdam, The Netherlands, October 11–14, 2016, Proceedings, Part V 14*, pages 561–578. Springer, 2016. 1, 2
- [7] Zhongang Cai, Mingyuan Zhang, Jiawei Ren, Chen Wei, Daxuan Ren, Zhengyu Lin, Haiyu Zhao, Lei Yang, Chen Change Loy, and Ziwei Liu. Playing for 3d human recovery. *IEEE Transactions on Pattern Analysis and Machine Intelligence*, 2024. 5, 8
- [8] Chi-Min Chan, Weize Chen, Yusheng Su, Jianxuan Yu, Wei Xue, Shanghang Zhang, Jie Fu, and Zhiyuan Liu. Chateval: Towards better llm-based evaluators through multi-agent debate. *arXiv preprint arXiv:2308.07201*, 2023. 2
- [9] Wei Cheng, Ruixiang Chen, Siming Fan, Wanqi Yin, Keyu Chen, Zhongang Cai, Jingbo Wang, Yang Gao, Zhengming Yu, Zhengyu Lin, et al. Dna-rendering: A diverse neural actor repository for high-fidelity human-centric rendering. In *Proceedings of the IEEE/CVF International Conference on Computer Vision*, pages 19982–19993, 2023. 5, 8
- [10] Paul F Christiano, Jan Leike, Tom Brown, Miljan Martic, Shane Legg, and Dario Amodei. Deep reinforcement learning from human preferences. *Advances in neural information processing systems*, 30, 2017. 2
- [11] Kevin Clark, Paul Vicol, Kevin Swersky, and David J Fleet. Directly fine-tuning diffusion models on differentiable rewards. In *The Twelfth International Conference on Learning Representations*, 2024. 2
- [12] Yann Dubois, Chen Xuechen Li, Rohan Taori, Tianyi Zhang, Ishaan Gulrajani, Jimmy Ba, Carlos Guestrin, Percy S Liang, and Tatsunori B Hashimoto. AlpacaFarm: A simulation framework for methods that learn from human feedback. *Advances in Neural Information Processing Systems*, 36:30039–30069, 2023. 2
- [13] Sai Kumar Dwivedi, Yu Sun, Priyanka Patel, Yao Feng, and Michael J Black. Tokenhmr: Advancing human mesh recovery with a tokenized pose representation. In *Proceedings of the IEEE/CVF Conference on Computer Vision and Pattern Recognition*, pages 1323–1333, 2024. 2
- [14] Ying Fan, Olivia Watkins, Yuqing Du, Hao Liu, Moonkyung Ryu, Craig Boutilier, Pieter Abbeel, Mohammad Ghavamzadeh, Kangwook Lee, and Kimin Lee. Dpok: Reinforcement learning for fine-tuning text-to-image diffusion models. *Advances in Neural Information Processing Systems*, 36:79858–79885, 2023. 2
- [15] Qi Fang, Kang Chen, Yinghui Fan, Qing Shuai, Jiefeng Li, and Weidong Zhang. Learning analytical posterior probability for human mesh recovery. In *Proceedings of the IEEE/CVF Conference on Computer Vision and Pattern Recognition*, pages 8781–8791, 2023. 2
- [16] Guérolé Fiche, Simon Leglaive, Xavier Alameda-Pineda, and Francesc Moreno-Noguer. Mega: Masked generative auto-encoder for human mesh recovery. In *Proceedings of the Computer Vision and Pattern Recognition Conference*, pages 5366–5378, 2025. 1, 2, 6
- [17] Lin Geng Foo, Jia Gong, Hossein Rahmani, and Jun Liu. Distribution-aligned diffusion for human mesh recovery. In *Proceedings of the IEEE/CVF International Conference on Computer Vision*, pages 9221–9232, 2023. 1, 6
- [18] Shubham Goel, Georgios Pavlakos, Jathushan Rajasegaran, Angjoo Kanazawa, and Jitendra Malik. Humans in 4d: Reconstructing and tracking humans with transformers. In *Proceedings of the IEEE/CVF International Conference on Computer Vision*, pages 14783–14794, 2023. 1, 2, 6
- [19] Daya Guo, Dejian Yang, Haowei Zhang, Junxiao Song, Ruoyu Zhang, Runxin Xu, Qihao Zhu, Shirong Ma, Peiyi Wang, Xiao Bi, et al. Deepseek-r1: Incentivizing reasoning capability in llms via reinforcement learning. *arXiv preprint arXiv:2501.12948*, 2025. 2
- [20] Jonathan Ho, Ajay Jain, and Pieter Abbeel. Denoising diffusion probabilistic models. *Advances in neural information processing systems*, 33:6840–6851, 2020. 3
- [21] Hui Huang, Xingyuan Bu, Hongli Zhou, Yingqi Qu, Jing Liu, Muyun Yang, Bing Xu, and Tiejun Zhao. An empirical study of llm-as-a-judge for llm evaluation: Fine-tuned judge model is not a general substitute for gpt-4. In *Findings of the Association for Computational Linguistics: ACL 2025*, pages 5880–5895, 2025. 2
- [22] Catalin Ionescu, Dragos Papava, Vlad Olaru, and Cristian Sminchisescu. Human3.6m: Large scale datasets and predictive methods for 3d human sensing in natural environments. *IEEE transactions on pattern analysis and machine intelligence*, 36(7):1325–1339, 2013. 5, 6, 7
- [23] Hanbyul Joo, Natalia Neverova, and Andrea Vedaldi. Exemplar fine-tuning for 3d human model fitting towards in-the-wild 3d human pose estimation. In *2021 International Conference on 3D Vision (3DV)*, pages 42–52. IEEE, 2021. 1, 2
- [24] Angjoo Kanazawa, Michael J Black, David W Jacobs, and Jitendra Malik. End-to-end recovery of human shape and

- pose. In *Proceedings of the IEEE conference on computer vision and pattern recognition*, pages 7122–7131, 2018. 2, 6
- [25] Angjoo Kanazawa, Jason Y Zhang, Panna Felsen, and Jitendra Malik. Learning 3d human dynamics from video. In *Proceedings of the IEEE/CVF conference on computer vision and pattern recognition*, pages 5614–5623, 2019. 6, 7
- [26] Seungone Kim, Jamin Shin, Yejin Cho, Joel Jang, Shayne Longpre, Hwaran Lee, Sangdoon Yun, Seongjin Shin, Sungdong Kim, James Thorne, et al. Prometheus: Inducing fine-grained evaluation capability in language models. In *The Twelfth International Conference on Learning Representations*, 2023. 2
- [27] Muhammed Kocabas, Chun-Hao P Huang, Joachim Tesch, Lea Müller, Otmar Hilliges, and Michael J Black. Spec: Seeing people in the wild with an estimated camera. In *Proceedings of the IEEE/CVF International Conference on Computer Vision*, pages 11035–11045, 2021. 5
- [28] Nikos Kolotouros, Georgios Pavlakos, Dinesh Jayaraman, and Kostas Daniilidis. Probabilistic modeling for human mesh recovery. In *Proceedings of the IEEE/CVF international conference on computer vision*, pages 11605–11614, 2021. 1, 2, 6
- [29] Christoph Lassner, Javier Romero, Martin Kiefel, Federica Bogo, Michael J Black, and Peter V Gehler. Unite the people: Closing the loop between 3d and 2d human representations. In *Proceedings of the IEEE conference on computer vision and pattern recognition*, pages 6050–6059, 2017. 2, 5
- [30] Dawei Li, Bohan Jiang, Liangjie Huang, Alimohammad Beigi, Chengshuai Zhao, Zhen Tan, Amrita Bhattacharjee, Yuxuan Jiang, Canyu Chen, Tianhao Wu, et al. From generation to judgment: Opportunities and challenges of llm-as-a-judge. In *Proceedings of the 2025 Conference on Empirical Methods in Natural Language Processing*, pages 2757–2791, 2025. 2
- [31] Jiefeng Li, Chao Xu, Zhicun Chen, Siyuan Bian, Lixin Yang, and Cewu Lu. Hybrik: A hybrid analytical-neural inverse kinematics solution for 3d human pose and shape estimation. In *Proceedings of the IEEE/CVF conference on computer vision and pattern recognition*, pages 3383–3393, 2021. 2, 3, 6
- [32] Shufan Li, Konstantinos Kallidromitis, Akash Gokul, Yusuke Kato, and Kazuki Kozuka. Aligning diffusion models by optimizing human utility. *Advances in Neural Information Processing Systems*, 37:24897–24925, 2024. 2
- [33] Tianle Li, Wei-Lin Chiang, Evan Frick, Lisa Dunlap, Tianhao Wu, Banghua Zhu, Joseph E Gonzalez, and Ion Stoica. From crowdsourced data to high-quality benchmarks: Arena-hard and benchbuilder pipeline. *arXiv preprint arXiv:2406.11939*, 2024. 2
- [34] Zhanhao Liang, Yuhui Yuan, Shuyang Gu, Bohan Chen, Tiankai Hang, Mingxi Cheng, Ji Li, and Liang Zheng. Aesthetic post-training diffusion models from generic preferences with step-by-step preference optimization. In *Proceedings of the Computer Vision and Pattern Recognition Conference*, pages 13199–13208, 2025. 2
- [35] Tsung-Yi Lin, Michael Maire, Serge Belongie, James Hays, Pietro Perona, Deva Ramanan, Piotr Dollár, and C Lawrence Zitnick. Microsoft coco: Common objects in context. In *Computer Vision—ECCV 2014: 13th European Conference, Zurich, Switzerland, September 6–12, 2014, Proceedings, Part V 13*, pages 740–755. Springer, 2014. 5
- [36] Jie Liu, Gongye Liu, Jiajun Liang, Yangguang Li, Jiaheng Liu, Xintao Wang, Pengfei Wan, Di Zhang, and Wanli Ouyang. Flow-grpo: Training flow matching models via online rl. *arXiv preprint arXiv:2505.05470*, 2025. 2
- [37] Matthew Loper, Naureen Mahmood, Javier Romero, Gerard Pons-Moll, and Michael J Black. Smpl: a skinned multi-person linear model. *ACM Transactions on Graphics (TOG)*, 34(6):1–16, 2015. 3
- [38] Cheng Lu, Yuhao Zhou, Fan Bao, Jianfei Chen, Chongxuan Li, and Jun Zhu. Dpm-solver: A fast ode solver for diffusion probabilistic model sampling in around 10 steps. *Advances in neural information processing systems*, 35:5775–5787, 2022. 2
- [39] Dushyant Mehta, Helge Rhodin, Dan Casas, Pascal Fua, Oleksandr Sotnychenko, Weipeng Xu, and Christian Theobalt. Monocular 3d human pose estimation in the wild using improved cnn supervision. In *2017 international conference on 3D vision (3DV)*, pages 506–516. IEEE, 2017. 5
- [40] Priyanka Patel and Michael J Black. Camerahr: Aligning people with perspective. In *2025 International Conference on 3D Vision (3DV)*, pages 1562–1571. IEEE, 2025. 1, 2, 6
- [41] Georgios Pavlakos, Vasileios Choutas, Nima Ghorbani, Timo Bolkart, Ahmed AA Osman, Dimitrios Tzionas, and Michael J Black. Expressive body capture: 3d hands, face, and body from a single image. In *Proceedings of the IEEE/CVF conference on computer vision and pattern recognition*, pages 10975–10985, 2019. 1, 2, 3
- [42] Zhen Qin, Rolf Jagerman, Kai Hui, Honglei Zhuang, Junru Wu, Le Yan, Jiaming Shen, Tianqi Liu, Jialu Liu, Donald Metzler, et al. Large language models are effective text rankers with pairwise ranking prompting. In *Findings of the Association for Computational Linguistics: NAACL 2024*, pages 1504–1518, 2024. 2
- [43] Alec Radford, Jong Wook Kim, Chris Hallacy, Aditya Ramesh, Gabriel Goh, Sandhini Agarwal, Girish Sastry, Amanda Askell, Pamela Mishkin, Jack Clark, et al. Learning transferable visual models from natural language supervision. In *International conference on machine learning*, pages 8748–8763. PMLR, 2021. 4
- [44] Rafael Rafailov, Archit Sharma, Eric Mitchell, Christopher D Manning, Stefano Ermon, and Chelsea Finn. Direct preference optimization: Your language model is secretly a reward model. *Advances in Neural Information Processing Systems*, 36, 2024. 2, 5
- [45] István Sáráandi and Gerard Pons-Moll. Neural localizer fields for continuous 3d human pose and shape estimation. *Advances in Neural Information Processing Systems*, 37: 140032–140065, 2024. 1, 2
- [46] Akash Sengupta, Ignas Budvytis, and Roberto Cipolla. Hierarchical kinematic probability distributions for 3d human shape and pose estimation from images in the wild. In *Proceedings of the IEEE/CVF international conference on computer vision*, pages 11219–11229, 2021. 6

- [47] Akash Sengupta, Ignas Budvytis, and Roberto Cipolla. Humaniflow: Ancestor-conditioned normalising flows on so (3) manifolds for human pose and shape distribution estimation. In *Proceedings of the IEEE/CVF Conference on Computer Vision and Pattern Recognition*, pages 4779–4789, 2023. 1, 6
- [48] Shreya Shankar, JD Zamfirescu-Pereira, Björn Hartmann, Aditya Parameswaran, and Ian Arawjo. Who validates the validators? aligning llm-assisted evaluation of llm outputs with human preferences. In *Proceedings of the 37th Annual ACM Symposium on User Interface Software and Technology*, pages 1–14, 2024. 2
- [49] Zhihong Shao, Peiyi Wang, Qihao Zhu, Runxin Xu, Junxiao Song, Xiao Bi, Haowei Zhang, Mingchuan Zhang, YK Li, et al. Deepseekmath: Pushing the limits of mathematical reasoning in open language models. *arXiv preprint arXiv:2402.03300*, 2024. 2, 3
- [50] Wenhao Shen, Wanqi Yin, Xiaofeng Yang, Cheng Chen, Chaoyue Song, Zhongang Cai, Lei Yang, Hao Wang, and Guosheng Lin. Adhmr: Aligning diffusion-based human mesh recovery via direct preference optimization. *arXiv preprint arXiv:2505.10250*, 2025. 1, 2, 4, 5, 6, 7, 8
- [51] Jiaming Song, Chenlin Meng, and Stefano Ermon. Denoising diffusion implicit models. *arXiv preprint arXiv:2010.02502*, 2020. 2, 3
- [52] Yang Song, Jascha Sohl-Dickstein, Diederik P Kingma, Abhishek Kumar, Stefano Ermon, and Ben Poole. Score-based generative modeling through stochastic differential equations. In *International Conference on Learning Representations*, 2021. 3
- [53] Anastasis Sathopoulos, Ligong Han, and Dimitris Metaxas. Score-guided diffusion for 3d human recovery. In *Proceedings of the IEEE/CVF Conference on Computer Vision and Pattern Recognition*, pages 906–915, 2024. 6
- [54] Pat Verga, Sebastian Hofstatter, Sophia Althammer, Yixuan Su, Aleksandra Piktus, Arkady Arkhangorodsky, Minjie Xu, Naomi White, and Patrick Lewis. Replacing judges with juries: Evaluating llm generations with a panel of diverse models. *arXiv preprint arXiv:2404.18796*, 2024. 2
- [55] Timo Von Marcard, Roberto Henschel, Michael J Black, Bodo Rosenhahn, and Gerard Pons-Moll. Recovering accurate 3d human pose in the wild using imus and a moving camera. In *Proceedings of the European conference on computer vision (ECCV)*, pages 601–617, 2018. 5, 6, 7
- [56] Bram Wallace, Meihua Dang, Rafael Rafailov, Linqi Zhou, Aaron Lou, Senthil Purushwalkam, Stefano Ermon, Caoming Xiong, Shafiq Joty, and Nikhil Naik. Diffusion model alignment using direct preference optimization. In *Proceedings of the IEEE/CVF Conference on Computer Vision and Pattern Recognition*, pages 8228–8238, 2024. 2, 5
- [57] Wenjia Wang, Yongtao Ge, Haiyi Mei, Zhongang Cai, Qingping Sun, Yanjun Wang, Chunhua Shen, Lei Yang, and Taku Komura. Zolly: Zoom focal length correctly for perspective-distorted human mesh reconstruction. In *Proceedings of the IEEE/CVF International Conference on Computer Vision*, pages 3925–3935, 2023. 6
- [58] Yidong Wang, Yunze Song, Tingyuan Zhu, Xuanwang Zhang, Zhuohao Yu, Hao Chen, Chiyu Song, Qiufeng Wang, Cunxiang Wang, Zhen Wu, et al. Trustjudge: Inconsistencies of llm-as-a-judge and how to alleviate them. *arXiv preprint arXiv:2509.21117*, 2025. 2
- [59] Yufu Wang, Yu Sun, Priyanka Patel, Kostas Daniilidis, Michael J Black, and Muhammed Kocabas. Prompthmr: Promptable human mesh recovery. In *Proceedings of the Computer Vision and Pattern Recognition Conference*, pages 1148–1159, 2025. 1, 2, 6
- [60] Jiazheng Xu, Xiao Liu, Yuchen Wu, Yuxuan Tong, Qinkai Li, Ming Ding, Jie Tang, and Yuxiao Dong. Imagereward: Learning and evaluating human preferences for text-to-image generation. *Advances in Neural Information Processing Systems*, 36, 2024. 2
- [61] Yuan Xu, Xiaoxuan Ma, Jiajun Su, Wentao Zhu, Yu Qiao, and Yizhou Wang. Scorehypo: Probabilistic human mesh estimation with hypothesis scoring. In *Proceedings of the IEEE/CVF Conference on Computer Vision and Pattern Recognition*, pages 979–989, 2024. 1, 2, 3, 5, 6, 7, 8
- [62] Zeyue Xue, Jie Wu, Yu Gao, Fangyuan Kong, Lingting Zhu, Mengzhao Chen, Zhiheng Liu, Wei Liu, Qiushan Guo, Weilin Huang, et al. Dancegrpo: Unleashing grpo on visual generation. *arXiv preprint arXiv:2505.07818*, 2025. 2
- [63] Kai Yang, Jian Tao, Jiafei Lyu, Chunjiang Ge, Jiabin Chen, Weihang Shen, Xiaolong Zhu, and Xiu Li. Using human feedback to fine-tune diffusion models without any reward model. In *Proceedings of the IEEE/CVF Conference on Computer Vision and Pattern Recognition*, pages 8941–8951, 2024. 2
- [64] Yifei Yin, Chen Guo, Manuel Kaufmann, Juan Jose Zarate, Jie Song, and Otmar Hilliges. Hi4d: 4d instance segmentation of close human interaction. In *Proceedings of the IEEE/CVF Conference on Computer Vision and Pattern Recognition*, pages 17016–17027, 2023. 5
- [65] Guangtao Zhai and Xionghuo Min. Perceptual image quality assessment: a survey. *Science China Information Sciences*, 63:1–52, 2020. 7
- [66] Bang Zhang, Ruotian Ma, Qingxuan Jiang, Peisong Wang, Jiaqi Chen, Zheng Xie, Xingyu Chen, Yue Wang, Fanghua Ye, Jian Li, et al. Sentient agent as a judge: Evaluating higher-order social cognition in large language models. *arXiv preprint arXiv:2505.02847*, 2025. 2
- [67] Hongwen Zhang, Yating Tian, Xinchu Zhou, Wanli Ouyang, Yebin Liu, Limin Wang, and Zhenan Sun. Pymaf: 3d human pose and shape regression with pyramidal mesh alignment feedback loop. In *Proceedings of the IEEE/CVF International Conference on Computer Vision*, pages 11446–11456, 2021. 6
- [68] Ce Zheng, Xianpeng Liu, Guo-Jun Qi, and Chen Chen. Potter: Pooling attention transformer for efficient human mesh recovery. In *Proceedings of the IEEE/CVF Conference on Computer Vision and Pattern Recognition*, pages 1611–1620, 2023. 6
- [69] Lianghai Zhu, Xinggang Wang, and Xinlong Wang. Judgelm: Fine-tuned large language models are scalable judges. *arXiv preprint arXiv:2310.17631*, 2023. 2